Journal of Magnetic Resonance 211 (2011) 109–113

Contents lists available at ScienceDirect

Journal of Magnetic Resonance

journal homepage: www.elsevier.com/locate/jmr

Multi-band frequency encoding method for metabolic imaging with hyperpolarized [1-^{13}C]pyruvate

Cornelius von Morze *, Galen Reed, Peter Shin, Peder E.Z. Larson, Simon Hu, Robert Bok, Daniel B. Vigneron

Department of Radiology and Biomedical Imaging, University of California, San Francisco, United States

ARTICLE INFO

Article history:
Received 10 December 2010
Revised 25 April 2011
Available online 1 May 2011

Keywords:
Hyperpolarized
C13
Preclinical
MRSI
TRAMP

ABSTRACT

A new method was developed for simultaneous spatial localization and spectral separation of multiple compounds based on a single echo, by designing the acquisition to place individual compounds in separate frequency encoding bands. This method was specially designed for rapid and robust metabolic imaging of hyperpolarized ^{13}C substrates and their metabolic products, and was investigated in phantom studies and studies in normal mice and transgenic models of prostate cancer to provide rapid metabolic imaging of hyperpolarized [1-^{13}C]pyruvate and its metabolic products [1-^{13}C]lactate and [1-^{13}C]alanine at spatial resolutions up to 3 mm in-plane. Elevated pyruvate and lactate signals in the vicinity of prostatic tissues were observed in transgenic tumor mice. The multi-band frequency encoding technique enabled rapid metabolic imaging of hyperpolarized ^{13}C compounds with important advantages over prior approaches, including less complicated acquisition and reconstruction methods.

1. Introduction

Hyperpolarized ^{13}C imaging provides >10,000 fold signal enhancement for detecting uptake of endogenous, nontoxic ^{13}C-labeled probes such as pyruvate, and their enzymatic conversion through key biochemical pathways [1–4]. Hyperpolarization lifts the prior constraint of poor sensitivity in MR metabolic imaging, but challenges the design of optimal acquisition strategies by requiring rapid sampling of spatial and chemical shift information of multiple ^{13}C resonances. To address these requirements for hyperpolarized MR, specialized pulse sequences have been developed with the capability to image multiple compounds rapidly, in order to track the metabolism of hyperpolarized substrates *in vivo*. Prior approaches include "spectroscopic imaging" (MRSI) methods, characterized by high spectral resolution, such as chemical shift imaging (CSI) [3], echo planar spectroscopic imaging (EPSI) [5], and spiral CSI [6], as well as "imaging" approaches like multi-echo methods [7,8], and interleaved acquisition of individual metabolites by frequency-specific excitation [9]. In this project, we have developed an "imaging" method called multi-band frequency encoding (FE), which uses a single gradient echo for both localization and spectral separation. The method relies on wide spectral separation and is thus well suited for hyperpolarized ^{13}C applications.

By leveraging the large chemical shift between hyperpolarized ^{13}C resonances, this method allows metabolic imaging with comparable or faster speeds than prior fast MRSI approaches. At the same time, it avoids the complexity of fast MRSI acquisition schemes involving rapidly switching gradients and/or non-Cartesian k-space trajectories, and their associated reconstruction steps, without sacrificing readout efficiency [2,6]. In comparison to the interleaved frequency-specific approach, images are truly acquired simultaneously, which provides an important advantage for multi-compound studies [10]. This new imaging technique was tested through imaging of a multi-chamber ^{13}C phantom, and *in vivo* imaging of hyperpolarized [1-^{13}C]pyruvate and its metabolic products [1-^{13}C]lactate and [1-^{13}C]alanine in normal mice and transgenic models of prostate cancer. This work is a novel implementation of the same basic idea recently described by Mugler et al. for separating hyperpolarized ^{129}Xe images of gas and dissolved phases [11], and is conceptually similar to previous work by Weaver for simultaneous multislice ^{1}H imaging [12], in this case applied to metabolic imaging of distinct ^{13}C-labeled metabolites. A full development of the theory of the technique is also presented in this work.

2. Theory

In spectroscopic imaging, spin frequency in the rotating frame (ω) is modulated by a magnetic field gradient and chemical shift:

* Corresponding author. Address: Department of Radiology and Biomedical Imaging, University of California, San Francisco, 1700 Fourth Street, QB3 Building Suite 102, San Francisco, CA 94158, United States. Fax: +1 415 514 4451.
E-mail address: cornelius.vonmorze@ucsf.edu (C. von Morze).

1090-7807/$ - see front matter © 2011 Elsevier Inc. All rights reserved.
doi:10.1016/j.jmr.2011.04.007

$$\omega_i(x,t) = \gamma(\delta_i B_0 + G(t)\cdot x) \quad (1)$$

where γ is the gyromagnetic ratio, δ_i is the chemical shift of species i, B_0 is the main magnetic field strength, G is the gradient strength and x is the spin position In the multi-band frequency encoding technique, the readout gradient amplitude is set such that the minimum chemical shift separation among species present ($\Delta\delta_{\min}$) exceeds the gradient field difference across the FOV (i.e. $\Delta\delta_{\min}B_0 > G\cdot\mathrm{FOV}$), whereby unique modulation occurs for all species at all locations, allowing determination of all spectral-spatial components by FE. The FOV here is defined only as the true object FOV, not an extended version containing the entire frequency range. Following Fourier transformation, images corresponding to each spectral component appear side-by-side within different FE bands (Fig. 1). To measure all of these components, the readout filter is opened wider than the conventional imaging setting of $\gamma G\cdot\mathrm{FOV}$; instead, the minimum setting is

$$BW_{\mathrm{read}} = (\delta_{\max} - \delta_{\min} + \Delta\delta_{\min})\gamma B_0 \quad (2)$$

where $\delta_{\min}$ and $\delta_{\max}$ are the minimum and maximum chemical shifts among the chemical species present. Due to practical sequence considerations, the readout bandwidth is likely to be the smallest multiple of $\Delta\delta_{\min}\gamma B_0$ exceeding this minimum. During the reconstruction procedure, metabolite images are shifted along x to their proper locations, based on known chemical shift differences. For example, if the maximum value of G is used, the reconstruction shift for metabolite i is $(\delta_i - \delta_{\min})N/\Delta\delta_{\min}$ pixels (where N = number of pixels across the FOV).

While in conventional imaging the readout gradient strength is usually maximized in order to minimize distortion (and also, to maximize imaging speed), in this method it is typically much lower than maximum. This is acceptable as long as the degree of misregistration and blurring remain small, and the imaging time remains sufficiently short.

The maximum FE bandwidth per pixel depends on the resolution and the minimum chemical shift separation:

$$BW_{\mathrm{pixel,\,max}} = \frac{\gamma\Delta\delta_{\min}B_0}{N} \quad (3)$$

which is also equal to the inverse of the minimum readout time for full Fourier sampling, determining the minimum TE and TR (and thus total scan time). B_0 misregistration (i.e. in mm per ppm inhomogeneity) scales with $\mathrm{FOV}/\Delta\delta_{\min}$. In this initial implementation for animal experiments as detailed below, the maximum misregistration due to a typical inhomogeneity of ±0.25 ppm is ±1 mm or one-third of a voxel.

If the T_2^* relaxation time is on the order of or less than the duration of the readout window, T_2^* blurring may occur along the readout direction, which could reduce the true spatial resolution in this dimension, and there could also be degradation of SNR. The corresponding k-space filter, which combines this asymmetric exponential decay filter with symmetric windowed sampling of the Fourier data [13], is

$$H_{T_2^*,\mathrm{wind}}(k) = e^{-TE/T_2^*}e^{-k/\gamma GT_2^*}\mathrm{rect}(k/W) \quad (4)$$

where W is the width of the spatial frequency sampling window, and the function "rect" is defined as a boxcar function equal to 1 when the argument lies between $-1/2$ and 1/2, and 0 otherwise. After inverse Fourier transformation (see A. Appendix), the point spread function is

$$h_{T_2^*,\mathrm{wind}}(x) = e^{-TE/T_2^*}\frac{e^{\tau_{\mathrm{read}}/2T_2^* - j\pi x/\Delta x} - e^{-\tau_{\mathrm{read}}/2T_2^* - j\pi x/\Delta x}}{\tau_{\mathrm{read}}\Delta x/T_2^* - 2\pi jx} \quad (5)$$

where Δx is the nominal spatial resolution (equal to 1/W), and T_{read} is the readout time (equal to $\mathrm{W}/\gamma\mathrm{G}$). To assess the extent of this effect on the experiments described in this study, this function was computed (Methods) over a range of reasonable representative values of T_2^*, and resultant loss of spatial resolution and SNR were estimated.

This method has not been applied for ^{1}H spectroscopic imaging because it would result in excessive distortion due to low FE bandwidth in the presence of B_0 inhomogeneity. Much larger minimum chemical shift separation in many ^{13}C applications should allow much higher spatial resolution, pixel bandwidth, and imaging speed with this method for ^{13}C. Comparing the minimum spectral separation for ^{1}H MRSI of the brain (choline-creatine, 0.2 ppm) to hyperpolarized ^{13}C studies of [1-^{13}C]pyruvate (pyruvate–alanine, 5.7 ppm), pixel misregistration due to a fixed ppm difference in B_0 would be 28x lower for ^{13}C (e.g. for a 4 cm FOV, misregistration due to 0.1 ppm inhomogeneity is 20 mm for ^{1}H vs. just 0.7 mm for ^{13}C), and the scan time is also 7 times faster.

3. Methods

3.1. Phantom experiments

A cylindrical multi-chamber phantom (d = 5.6 cm) containing [1-^{13}C]pyruvate, [1-^{13}C]alanine, and [1-^{13}C]lacate in three separate internal spheres, respectively, was scanned in a 3T GE human scanner equipped with a custom built transmit-receive dual-tuned ^{1}H/^{13}C coil designed for imaging rats (d = 8 cm, length = 9 cm, ^{13}C channel- quadrature, ^{1}H channel–linear only). The pulse sequence was a single slice axial 2D spoiled gradient echo (SPGR) acquisition designed for resolution of pyruvate and its metabolic products lactate and alanine. The chemical shifts were determined from a separate non-localized MRS scan. A 32-point readout of total bandwidth = 0.74 kHz was used. The first two eight-point bands

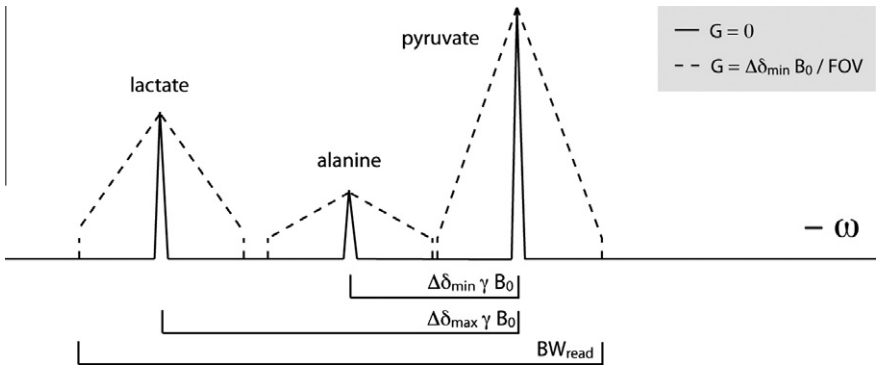

Fig. 1. Schematic representation of multi-band frequency encoding method, showing spread of metabolite signals into adjacent, non-overlapping frequency bands used for spatial encoding, when a correctly chosen frequency encoding gradient is activated. All quantities are as defined in the text.

represented pyruvate and alanine, with lactate extending into the remaining two bands. The spatial resolution was 7.5 mm in-plane by 20 mm slice (1.13 cm^3). The other parameters were: flip angle = 20°, TE/TR = 26 ms/58 ms (T_{read} = 44 ms with G_{read} = 0.029 G/cm, $G_{slice\ select}$ = 0.58 G/cm), FOV = 6 cm (AP, frequency) × 12 cm (RL, phase), acquisition matrix = 32 × 16, NEX = 160, scan time per NEX = 928 ms.

3.2. Animal experiments

The distribution and metabolism of hyperpolarized [1-^{13}C]pyruvate was imaged in one normal mouse and two transgenic mice with prostate cancer (transgenic adenocarcinoma of the mouse prostate, or TRAMP) [14]. Each sample (24 μL or ~30 mg) of 99% [1-^{13}C]pyruvate mixed with trityl radical OX063 (GE Healthcare, Oslo, Norway) was loaded into the 3.35T magnet of the HyperSense polarizer (Oxford Instruments Biotools, Oxford, UK), where it was cooled to 1.3 K and irradiated by microwaves @ 94.117 GHz for approximately 1 h. The sample was then removed from the magnet and rapidly dissolved in a heated solution of 4.6 mL TRIS/NaOH buffer, resulting in a ~80 mM solution of pH ~7.5. After rapidly transporting the solution to the scanner room, the mice were intravenously injected with a bolus of 350 μL over 12 s, followed by a 150 μL saline flush. The polarization of an aliquot taken from the dissolved sample was measured in a low field spectrometer.

A single stack of eight axial slices extending from the prostate to the liver was acquired at 35 s after the start of the injection. *In vivo* chemical shifts differed slightly from the phantom in their absolute values, and were determined from previously acquired MRS data (ω_{pyr} = 32,131,400 ∗ 2π rad/sec, $\Delta\delta_{pyr\text{-}ala}$ = 5.7 ppm, $\Delta\delta_{ala\text{-}lac}$ = 6.6 ppm). The spatial resolution was 3 mm in-plane by 5 mm slice (0.045 cm^3). The imaging parameters were as described above except: FOV = 2.4 cm (AP, frequency) × 4.8 cm (RL, phase), G_{read} = 0.072 G/cm, $G_{slice\ select}$ = 2.34 G/cm, acquisition matrix = 32 × 16, scan time = 7.4 s. To maintain nearly constant transverse magnetization following each RF pulse, the flip angle was increased over the phase encoding steps for each slice according to $\theta(n) = \arctan(\sin(\theta(n+1))$, with the last pulse being 90° [15]. A syringe containing a solution of enriched [^{13}C]lactate (1.77 M) was placed in the coil along with each mouse in order to calibrate the transmit gain prior to the experiment. In this case the RF coil was a quadrature transmit-receive dual-tuned ^{1}H/^{13}C coil designed for imaging mice (d = 5 cm, length = 8 cm).

3.3. Post-processing

The transmit RF pulse was centered on the pyruvate frequency. For relatively thin 2D slices, some small chemical shift misregistration of the RF pulse profiles occurs. The RF pulse bandwidth was 1250 Hz, resulting in shifted transmit profiles for alanine (shifted by ~0.7 mm) and lactate (~1.6 mm). In post-processing, the alanine and lactate data were interpolated, shifted, and resampled to realign the data along z. Even after correction, a consequence of the misregistration is that one edge slice has incomplete alanine and lactate signal.

A small signal from pyruvate hydrate, centered between the alanine and lactate bands, resulted in slight contamination of the alanine band, and to a lesser extent, the lactate band. The contamination was reduced by applying knowledge of the pyruvate signal to estimate a minimum pyruvate hydrate signal level at physiological pH (5% of the pyruvate signal, based on previous MRSI studies), which was subtracted from the appropriate locations in the alanine and lactate bands. Finally, interpolated metabolite images (64 × 64 for each metabolite) were overlaid onto standard axial multi-slice T_2-weighted ^{1}H FSE images acquired with identical graphic prescription.

3.4. Simulations

Simulations were conducted to assess the potential extent of T_2^* blurring and loss of SNR. The T_2 relaxation times of the ^{13}C nuclei of interest are relatively long, in the hundreds of milliseconds. We derived T_2^* relaxation times from a previous study in which T_2 relaxation times were measured [16], taking the shortest T_2 value measured (380 ms for alanine in normal rat liver) and adjusting downward up to a factor of 10 for varying levels of intravoxel inhomogeneity (T_2^* = 380 ms, 125 ms, 38 ms, and for comparison, infinite). The point spread function (Eq. (5)) was calculated for each of these T_2^* values, and the FWHM of each function was measured and compared to the ideal value for infinite relaxation time to determine degradation of spatial resolution, and the integral of each function in the FWHM portion was taken as an estimate of the relative SNR.

4. Results

Shifting the lactate and alanine sub-images by amounts corresponding to their *in vivo* chemical shifts as measured in previous

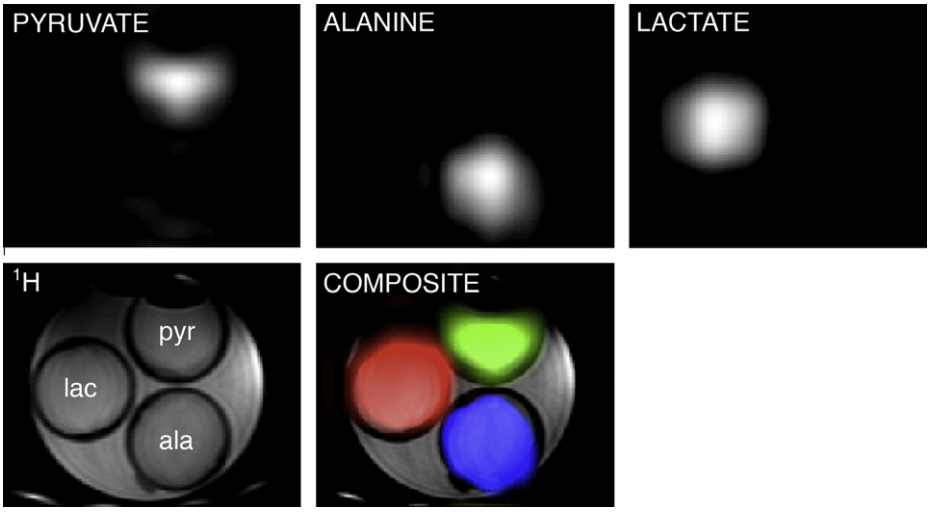

Fig. 2. Axial imaging of a cylindrical multi-chamber ^{13}C phantom (d = 5.6 cm) with internal spheres (d = 2.3 cm) containing enriched ^{13}C-pyruvate, -alanine, and -lactate. Nominal spatial resolution of ^{13}C image acquisition was 7.5 mm in-plane. Top row: Individual reconstructed ^{13}C metabolite images. Bottom row: ^{1}H FSE image and composite image overlay.

MRSI studies resulted in excellent co-registration of all image sets (Fig. 2- multi-chamber phantom, Fig. 3- *in vivo*). For each metabolite, exactly the same shift was applied across all slices in the data sets. The small pyruvate hydrate signal was effectively filtered from the alanine and lactate bands by the described method. The polarization of the injected pyruvate was ~25%, as measured by the spectrometer.

In all three animals (Figs. 4 and 5), the largest hyperpolarized signals were observed in the kidneys and liver, with alanine mostly localized to the liver. Both transgenic prostate cancer mice had regions of T_2-weighted signal changes in the anatomic region just surrounding and superior to the urethra, which is the site of early tumor development in the TRAMP model [17]. The mean tumor lactate-to-pyruvate ratios in both mice, 1.32 for one mouse with a large periurethral gross tumor (d_{max} = 1.5 cm), and 0.64 for the other mouse with a smaller tumor (d_{max} = 1.0 cm), were elevated over the ratio in the prostatic region of the normal mouse (0.49). In the smaller tumor, pyruvate was largest in the periphery, around a centralized region of lower pyruvate and high lactate.

The qualitative appearance of the results in Figs. 2 and 3 indicate that the resolution of the acquisitions were not seriously degraded by T_2^* blurring. It is important to note that although the resolution of the phantom scan was lower than the animal scans due to much lower SNR, the readout duration was the same, so the percent degradation of spatial resolution from the nominal value due to T_2^* blurring would be the same (from Eq. (5)). Results of the simulations of T_2^* blurring and SNR loss are shown in Fig. 6 in the plots of the point spread function. Increases in the FWHM of the point spread function from its ideal value (for infinite T_2^*, FWHM = 3.616 mm) were negligible for T_2^* values of 380 ms (3.622 mm) and 125 ms (3.638 mm). The expected degradation in spatial resolution was 5.4% for $T_2^* = 38$ ms (3.810 mm), based on comparing the FWHM values. The relative SNR values measured by integrating under the FWHM area were 94% (380 ms), 82% (125 ms) and 56% (38 ms).

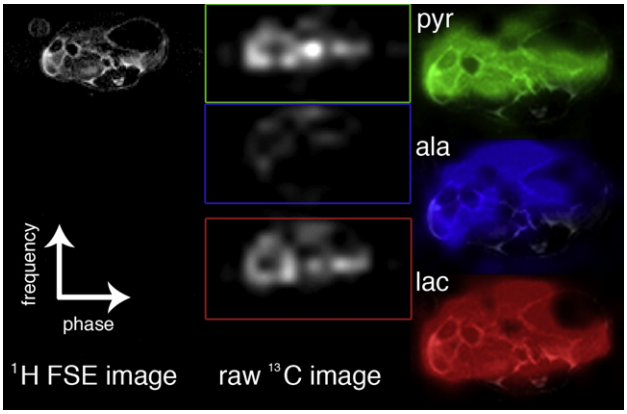

Fig. 3. Separation of pyruvate, alanine, and lactate images in a normal mouse by multi-band frequency encoding method. Nominal resolution was 3 mm in-plane by 5 mm slice. Liver slice was selected for high concentration of all three metabolites. Pyruvate image (green box) occupies top frequency encoding band in raw ^{13}C imaging data, with alanine (blue) and lactate (red) images below. Reconstructed composite image overlays shown at right. (For interpretation of the references to color in this figure legend, the reader is referred to the web version of this article.)

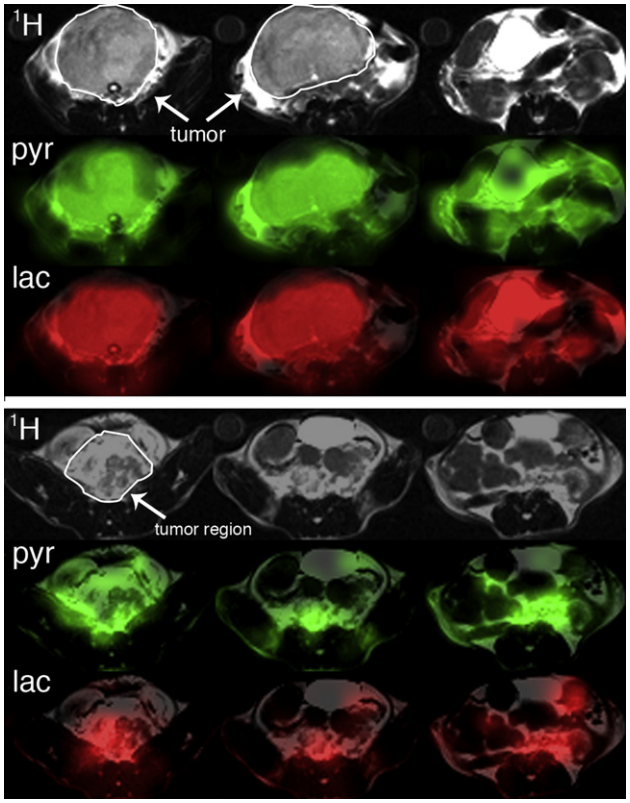

Fig. 5. Pelvic/abdominal metabolite distribution from two transgenic prostate cancer (TRAMP) mice imaged using multi-band frequency encoding. (left-to-right = inferior-to-superior). In the mouse at top, lactate is well localized to the region of gross tumor as defined on T2w ^{1}H images.

5. Discussion

In this project we developed a new, robust method for imaging of multiple ^{13}C compounds widely separated in chemical shift and demonstrated its application for imaging hyperpolarized

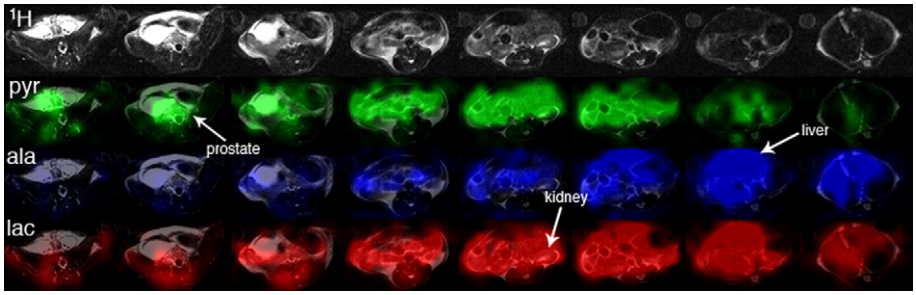

Fig. 4. Axial imaging of hyperpolarized [1-^{13}C]pyruvate and its metabolic products by multi-band frequency encoding in a normal mouse. All individual metabolite images from stack are shown, overlaid on co-registered T2w ^{1}H images, with anatomic landmarks. Alanine signal is mostly localized to the liver, due to highest expression of alanine transaminase.

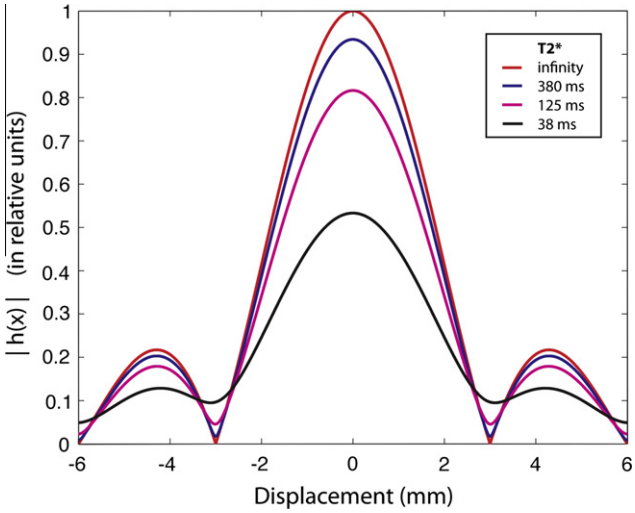

Fig. 6. Plots of point spread function for multi-band frequency encoding imaging method (Eq. (5)) as described for animal experiments, including effects of T_2^* blurring and symmetric windowed Fourier sampling, computed for various possible T_2^* values to reflect different levels of intravoxel inhomogeneity. Red – infinite, blue – 380 ms, magenta – 125 ms, black – 38 ms. (For interpretation of the references to color in this figure legend, the reader is referred to the web version of this article.)

[1-^{13}C]pyruvate and its metabolic products *in vivo*. In phantom scans and animal scans of normal mice and transgenic models of prostate cancer, identical shifts were applicable to all of the data (i.e. in all slices of all exams). This was expected due to the fact that very consistent chemical shifts have been robustly observed through prior *in vivo* MRSI studies. We successfully implemented a method for removing signal contamination resulting from overlap of a small pyruvate hydrate signal into the alanine and lactate bands. This method assumes that pyruvate hydrate signal adds in phase with lactate and alanine signals, which should be a reasonable assumption. A situation could arise where a small difference in the B_0 field between the aliased spatial positions may put the signals out of phase. In any case, the levels of pyruvate hydrate are quite small in comparison to lactate at 35 s after injection, but this could be a problem for dynamic studies. B_0 misregistration was estimated to be minor for the described application, and this was corroborated by good alignment of the experimental data with ^{1}H images. If misregistration were increased in a different application or experimental conditions of poor shim, misregistration could also be corrected based on a B_0 map, and the same correction could be applied to all images as they all have the same misregistration.

Higher spatial resolution and faster acquisition times are facilitated by larger minimum chemical shift separation. Another application that could benefit is imaging of pH using hyperpolarized [^{13}C]bicarbonate [18], in which bicarbonate and CO_2 are separated by 36 ppm. Similarly, more advanced RF methods such as suppression pulses for alanine or multi-band excitation of pyruvate and lactate could be utilized to localize just these components for better performance than demonstrated in this study.

Appendix A

Derivation of point spread function Eq. (5) from Eq. (4):

$$h(x) = FT^{-1}\{H(k)\} = \int_{-\infty}^{\infty} e^{-TE/T_2^*} e^{-k/\gamma G T_2^*} \mathrm{rect}(k/W) e^{2\pi jxk}\, dk$$

$$= e^{-TE/T_2^*} \int_{-W/2}^{W/2} e^{-k/\gamma G T_2^*} e^{2\pi jxk} dk = e^{-TE/T_2^*} \int_{-W/2}^{W/2} e^{k(2\pi jx - 1/\gamma G T_2^*)}\, dk$$

$$= e^{-TE/T_2^*} \frac{1}{2\pi jx - 1/\gamma G T_2^*} e^{k(2\pi jx - 1/\gamma G T_2^*)} \Big|_{-W/2}^{W/2}$$

$$= e^{-TE/T_2^*} \frac{e^{(W/2)(2\pi jx - 1/\gamma G T_2^*)} - e^{-(W/2)(2\pi jx - 1/\gamma G T_2^*)}}{2\pi jx - 1/\gamma G T_2^*}$$

And since $\tau_{\mathrm{read}} = 1/(\gamma G \Delta x)$,

$$h(x) = e^{-TE/T_2^*} \frac{e^{(1/\Delta x)(\pi jx - \tau_{\mathrm{read}} \Delta x/2T_2^*)} - e^{-(1/\Delta x)(\pi jx - \tau_{\mathrm{read}} \Delta x/2T_2^*)}}{2\pi jx - \tau_{\mathrm{read}} \Delta x/T_2^*}$$

$$= e^{-TE/T_2^*} \frac{e^{\tau_{\mathrm{read}}/2T_2^* - j\pi x/\Delta x} - e^{-\tau_{\mathrm{read}}/2T_2^* - j\pi x/\Delta x}}{\tau_{\mathrm{read}} \Delta x/T_2^* - 2\pi jx}$$

References

[1] J.H. Ardenkjaer-Larsen, B. Fridlund, A. Gram, et al., Increase in signal-to-noise ratio of >10,000 times in liquid-state NMR, Proc. Natl. Acad. Sci. USA 100 (18) (2003) 10158–10163.

[2] A.P. Chen, M.J. Albers, C.H. Cunningham, et al., Hyperpolarized C-13 spectroscopic imaging of the TRAMP mouse at 3T-initial experience, Magnetic Resonance in Medicine: Official Journal of the Society of Magnetic Resonance in Medicine/Society of Magnetic Resonance in Medicine 58 (6) (2007) 1099–1106.

[3] K. Golman, R. In 't Zandt, M. Thaning, Real-time metabolic imaging, Proc. Natl. Acad. Sci. USA 103 (30) (2006) 11270–11275.

[4] M.A. Schroeder, L.E. Cochlin, L.C. Heather, K. Clarke, G.K. Radda, D.J. Tyler, In vivo assessment of pyruvate dehydrogenase flux in the heart using hyperpolarized carbon-13 magnetic resonance, Proc. Natl. Acad. Sci. USA 105 (33) (2008) 12051–12056.

[5] C.H. Cunningham, A.P. Chen, M.J. Albers, et al., Double spin-echo sequence for rapid spectroscopic imaging of hyperpolarized ^{13}C, J. Magn. Reson. 187 (2) (2007) 357–362.

[6] D. Mayer, Y.F. Yen, Y.S. Levin, et al., In vivo application of sub-second spiral chemical shift imaging (CSI) to hyperpolarized 13C metabolic imaging: comparison with phase-encoded CSI, J Magn Reson 204 (2) (2010) 340–345.

[7] J. Leupold, S. Mansson, J.S. Petersson, J. Hennig, O. Wieben, Fast multiecho balanced SSFP metabolite mapping of (1)H and hyperpolarized (13)C compounds, Magma 22 (4) (2009) 251–256.

[8] S.B. Reeder, J.H. Brittain, T.M. Grist, Y.F. Yen, Least-squares chemical shift separation for (13)C metabolic imaging, J. Magn. Reson. Imaging. 26 (4) (2007) 1145–1152.

[9] A.Z. Lau, A.P. Chen, N.R. Ghugre, V. Ramanan, W.W. Lam, K.A. Connelly, G.A. Wright, C.H. Cunningham, Rapid multislice imaging of hyperpolarized ^{13}C pyruvate and bicarbonate in the heart, Magn Reson Med. 64 (5) (2010) 1323–1331.

[10] D.M. Wilson, K.R. Keshari, P.E. Larson, et al., Multi-compound polarization by DNP allows simultaneous assessment of multiple enzymatic activities in vivo, J Magn Reson. 205 (2010) 141–147.

[11] J.P. Mugler 3rd, T.A. Altes, I.C. Ruset, et al., Simultaneous magnetic resonance imaging of ventilation distribution and gas uptake in the human lung using hyperpolarized xenon-129, Proc Natl Acad Sci USA 107 (50) (2010) 21707–21712.

[12] J.B. Weaver, Simultaneous multislice acquisition of MR images, Magn. Reson. Med. 8 (3) (1988) 275–284.

[13] E.M. Haacke, R.W. Brown, M.R. Thompson, R. Venkatesan, Magnetic resonance imaging: physical principles and sequence design, 1999, pp. 286.

[14] N.M. Greenberg, F. DeMayo, M.J. Finegold, et al., Prostate cancer in a transgenic mouse, Proc. Natl. Acad. Sci. USA 92 (8) (1995) 3439–3443.

[15] L. Zhao, R. Mulkern, C.H. Tseng, et al., Gradient-echo imaging considerations for hyperpolarized 129Xe MR, J. Magn. Reson. B 113 (2) (1996) 179–183.

[16] Y.F. Yen, P. Le Roux, D. Mayer, et al., T-2 relaxation times of C-13 metabolites in a rat hepatocellular carcinoma model measured in vivo using C-13-MRS of hyperpolarized [1-C-13]pyruvate, Nmr Biomed. 23 (4) (2010) 414–423.

[17] A. Degrassi, M. Russo, E. Scanziani, et al., Magnetic resonance imaging and histopathological characterization of prostate tumors in TRAMP mice as model for pre-clinical trials, Prostate 67 (4) (2007) 396–404.

[18] F.A. Gallagher, M.I. Kettunen, S.E. Day, et al., Magnetic resonance imaging of pH in vivo using hyperpolarized ^{13}C-labelled bicarbonate, Nature 453 (7197) (2008) 940–943.